THE JOURNAL OF PHYSICAL CHEMISTRY A

 VOLUME 106, NUMBER 47, NOVEMBER 28, 2002

ARTICLES

Photodissociation of Acetaldehyde, $CH_3CHO \rightarrow CH_4 + CO$: Direct ab Initio Dynamics Study

Yuzuru Kurosaki* and Keiichi Yokoyama

Advanced Photon Research Center, Japan Atomic Energy Research Institute, Umemidai, Kizu-cho, Soraku-gun, Kyoto 619-0215, Japan

Received: April 18, 2002; In Final Form: September 17, 2002

A total of 100 trajectories for the photodissociation, $CH_3CHO \rightarrow CH_4 + CO$, on the S_0 potential surface have been calculated using the direct ab initio molecular dynamics method at the RMP2(full)/cc-pVDZ level of theory. The energy distributions for the relative translational energy, the CO internal energy, and the CH_4 internal energy were calculated to be 28, 20, and 51%, respectively. It was predicted that the product CO is highly rotationally excited but vibrationally almost not excited; on average, the rotational and vibrational quantum numbers were 68.2 and 0.15, respectively, which qualitatively agrees with the recent observation of Gherman et al. (*J. Chem. Phys.* **2001**, *114*, 6128.)

1. Introduction

It is widely known that aldehydes such as formaldehyde and acetaldehyde are, in the ultraviolet (UV) region, excited to the singlet state (S_1) from the ground singlet state (S_0) through an n-π* transition.[1] Electronically excited aldehydes in the S_1 state decay to S_0 with a fluorescence emission or undergo photodissociation. Photodissociation of aldehydes is indirect because the C−O bond still remains strong after the n-π* transition. Several photodissociation channels of aldehydes in the S_1 state are possible. One of the channels goes through the intersystem crossing (ISC) between S_1 and the lowest triplet state (T_1) and the other the internal conversion (IC) from S_1 to highly vibrationally excited states of S_0. It has been established that the T_1 potential energy surface correlates to the radical products with a small reaction barrier and the ground S_0 surface to both the radical and molecular products with considerably higher barriers.

Photodissociation of formaldehyde has attracted both experimental[2] and theoretical[3] interest for more than two decades. It has been revealed that formaldehyde excited to the S_1 state is likely to undergo rapid IC to vibrationally excited levels of S_0. At a high photolysis energy the radical formation channel (H + HCO) is accessible, but below the threshold of this channel, photodissociation leads to the formation of a hydrogen molecule and carbon monoxide (H_2 + CO). In particular, the latter channel has been extensively studied in a series of experiments,[2] and detailed information on the product state distributions has been accumulated. Therefore, this molecular formation channel has been a typical test case for classical trajectory studies.[3e−j]

A lot of experimental[4] and theoretical[5] work has also been done for photodissociation of acetaldehyde, because this has been considered a key molecule in understanding the photochemistry of larger carbonyl compounds. It was observed that, at a low vibrational level, acetaldehyde in the S_1 state decays mainly to a highly vibrationally excited level of S_0 via IC between S_0 and S_1. For excitation wavelengths shorter than 317 nm, however, the dissociation channel to the CH_3 + HCO radicals via ISC between S_1 and T_1 opens; this radical channel has been shown to be the major dissociation process of acetaldehyde photolysis in the UV region. A number of laser-induced fluorescence (LIF) studies have strongly supported this

* Corresponding author. Tel.: +81-77-471-3400. Fax: +81-77-471-3316. E-mail: kurosaki@apr.jaeri.go.jp.

10.1021/jp020998f CCC: $22.00
Published on Web 11/05/2002

TABLE 1: Harmonic Vibrational Frequencies for the RMP2(full)/cc-pVDZ Geometries

	sym	frequency/cm^{-1}					ZPE/hartree
CH_3CHO	C_s	171 (a″)	504 (a′)	779 (a″)	908 (a′)	1133 (a″)	0.05611
		1137 (a′)	1376 (a′)	1433 (a′)	1461 (a′)	1476 (a″)	
		1802 (a′)	2949 (a′)	3090 (a′)	3185 (a′)	3226 (a′)	
CH_4	T_d	1339 (t_2)	1339 (t_2)	1339 (t_2)	1568 (e)	1568 (e)	0.04552
		3092 (a_1)	3245 (t_2)	3245 (t_2)	3245 (t_2)		
CO	$C_{\infty v}$	2117 (σ)					0.00482
TS	C_s	1798i (a′)	139 (a″)	261 (a′)	505 (a″)	535 (a′)	0.04929
		752 (a′)	933 (a″)	1070 (a′)	1427 (a″)	1432 (a′)	
		1845 (a′)	3059 (a′)	3194 (a′)	3215 (a″)	3266 (a′)	

radical decay channel; the fluorescence was found to disappear for excitation wavelengths shorter than 317 nm, indicating the opening of the radical channel through ISC.

At a sufficiently high energy, the rates of IC and ISC become comparable because of the increase in density of states.[1] Recently, Gherman et al.,[4n] using the vacuum UV LIF method, have examined the molecular $CH_4 + CO$ channel of acetaldehyde photodissociation at a wavelength of 248 nm. They have measured the vibrational and rotational state distributions of the product CO molecule; as a result, the CO was found to be highly rotationally excited, but no vibrationally excited CO was detected. The rotational temperature was estimated to be about 1300 K. They have also carried out ab initio calculations at the density functional theory level for the $CH_3CHO \rightarrow CH_4 + CO$ reaction on the S_0 surface. It was predicted that the reaction is exoergic by 1.7 kcal mol^{-1} and the barrier height is 81.1 kcal mol^{-1}. The vector of the imaginary vibrational mode for the transition state (TS) strongly suggested that the rotationally hot and vibrationally cold CO is produced, which is consistent with their experimental observation. In addition, they have obtained the RRKM rate constant $k(E)$ for this unimolecular dissociation using the calculated data.

In the present work, we theoretically investigate the $CH_4 +$ CO channel of acetaldehyde photodissociation, using the classical trajectory method. Here, we employ the ab initio direct molecular dynamics technique that is now becoming practical as a result of the rapid progress in computer technology.

2. Methods of Calculation

Geometries of stationary points for the $CH_3CHO \rightarrow CH_4 +$ CO reaction on the S_0 potential energy surface were fully optimized at the all-electron restricted second-order Møller−Plesset perturbation (RMP2(full))[6] level with the correlation-consistent polarized valence double-ζ (cc-pVDZ) basis set of Dunning.[7] Harmonic vibrational frequencies were computed analytically and the optimized geometries were characterized as minima or saddle points of the potential energy surface. Single-point energies were calculated using the all-electron restricted fourth-order MP method including single, double, triple, and quadruple electron excitations (RMP4(SDTQ,full))[8] and using the all-electron restricted quadratic configuration interaction method including single and double substitutions and perturbative triple substitutions (RQCISD(T,full)).[9] The intrinsic reaction coordinate (IRC)[10] was calculated at the RMP2(full)/cc-pVDZ level of theory, and it was confirmed that the reactant, TS, and products are connected with one another through a single reaction pathway. These ab initio molecular orbital calculations were performed using the GAUSSIAN 98 program package.[11]

Trajectories were started at the TS in the direction of the imaginary vibrational mode with the kinetic energy of 34.2 kcal mol^{-1}. This energy corresponds to the difference between the photolysis energy 248 nm[4n] and the theoretical barrier height 81.1 kcal mol^{-1} that has most recently been calculated at the B3LYP/cc-pVTZ(-f) level.[4n] Zero-point energies (ZPEs) were added to the remaining vibrational modes, the initial phases of which were selected randomly. The rotational temperature was set to 0 K. A total of 100 trajectories were integrated with the step size of 0.25 amu$^{1/2}$ bohr using the analytical Hessian[12] at the RMP2(full)/cc-pVDZ level of theory. For each trajectory, integration of 180 steps were done when the distance between the products CH_4 and CO was ∼6 Å. The total energy was conserved to 10^{-5} hartree. The average time for the trajectories was ∼80 fs. The trajectory calculations were carried out using the code implemented in the GAUSSIAN 98 program package.

TABLE 2: Total Energies for the RMP2(full)/cc-pVDZ Geometries (hartree)

	state	RMP2(full)/cc-pVDZ	RMP4(SDTQ,full)/cc-pVTZ	RQCISD(T,full)/cc-pVTZ
CH_3CHO	$^1A'$	−153.39351	−153.63483	−153.63165
CH_4	$^1A_1$	−40.36303	−40.45426	−40.45483
CO	$^1\Sigma^+$	−113.04085	−113.18638	−113.18097
TS	$^1A'$	−153.25253	−153.49792	−153.49227

3. Results and Discussion

A. Geometry and Energetics. In Tables 1 and 2 are given the harmonic vibrational frequencies at the RMP2(full)/cc-pVDZ level and the total energies at the RMP2(full)/cc-pVDZ, RMP4(SDTQ,full)/cc-pVTZ, and RQCISD(T,full)/cc-pVTZ levels for species in the $CH_3CHO \rightarrow CH_4 + CO$ reaction on the S_0 potential energy surface. In Table 3 are compared the calculated and experimental values for the relative energies of this reaction. It is seen that the barrier height calculated at the RMP2(full)/cc-pVDZ level in the present work is comparable with the barrier heights obtained at the RMP4(SDTQ,full)/cc-pVTZ and RQCISD(T,full)/cc-pVTZ levels and with those obtained using other high-level ab initio methods.[5a−c] Although the exothermicity predicted at the RMP2(full)/cc-pVDZ level in the present work is slightly larger than the G1,[5b] G2,[5c] B3LYP,[4n] RMP4, and RQCISD values and experiment, one thinks that the agreement is still good when one considers the employed inexpensive method and basis set. We therefore conclude that the ab initio MO method, RMP2(full)/cc-pVDZ, employed for the direct trajectory calculations is energetically quite reliable.

In Figure 1 are shown the optimized geometries for the reactant CH_3CHO and TS at the RMP2(full)/cc-pVDZ level. The vector of the imaginary vibrational mode is depicted in the TS geometry. Both the geometries have been predicted to have C_s symmetry and were confirmed to be at a minimum and saddle point on the potential energy surface, respectively, with the harmonic vibrational analyses presented in Table 1. We have found that the present RMP2(full)/cc-pVDZ geometries for CH_3CHO and the TS are comparable with those obtained with

TABLE 3: Relative Energies Estimated by Theory and Experiment (kcal mol^{-1})

method	CH_3CHO	TS	$CH_4 + CO$	ref
CISD+SCC/3-21G//HF/3-21G	0.0	84.6 (88.8)[a]	−10.9 (−7.3)	5a
G1	0.0	83.1 (86.3)	−6.8	5b
G2	0.0	82.9 (87.1)	−5.9[b]	5c
B3LYP/cc-pVTZ(-f)//B3LYP/6-31G**	0.0	81.1 (85.3)	(−1.7)	4n
RMP2(full)/cc-pVDZ//RMP2(full)/cc-pVDZ	0.0	84.2 (88.5)	−10.1 (−6.5)	present work
RMP4(SDTQ,full)/cc-pVTZ//RMP2(full)/cc-pVDZ	0.0	81.6 (85.9)	−7.3 (−3.6)	present work
RQCISD(T,full)/cc-pVTZ//RMP2(full)/cc-pVDZ	0.0	83.2 (87.5)	−6.2 (−2.6)	present work
experiment	0.0		−3.5	14

[a] In parentheses are given the values without the ZPE correction. [b] Reaction enthalpy at 298 K.

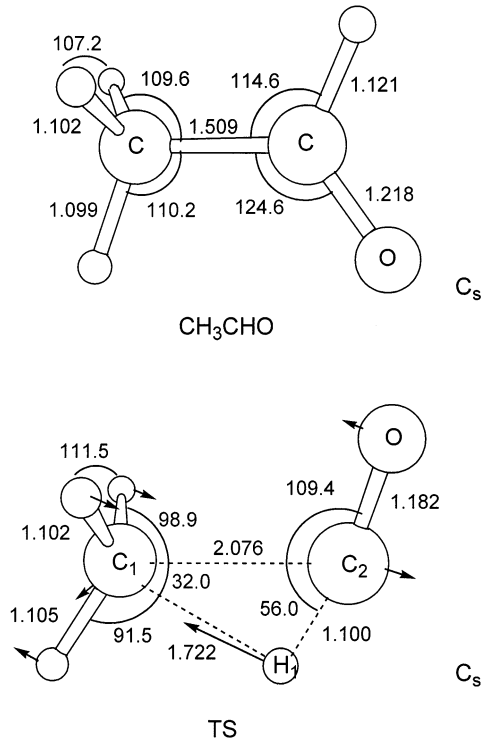

Figure 1. Optimized geometries for CH_3CHO and the TS at the RMP2(full)/cc-pVDZ level of theory. In the TS geometry is shown the vector of the imaginary vibrational mode. Bond lengths and angles are given in Å and degree, respectively.

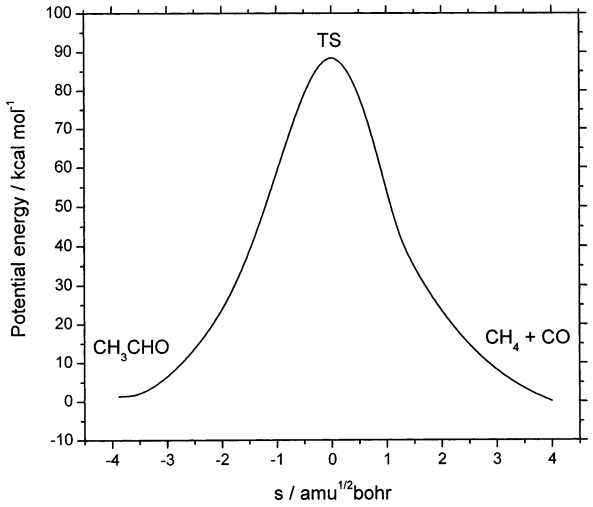

Figure 2. Potential energy profile along the IRC for the $CH_3CHO \rightarrow CH_4 + CO$ reaction.

other high-level ab initio methods[4n,5b,c] and experiment.[13] We have also found that the TS imaginary frequency, 1798i cm^{-1}, and its vector calculated in the present work agree well with the B3LYP/6-31G** result.[4n] The vector strongly suggests that the product CO is rotationally hot and vibrationally cold and one of the CH bonds of the product CH_4 is vibrationally hot, which will be discussed below.

Figure 2 shows the potential energy profile along the IRC for the $CH_3CHO \rightarrow CH_4 + CO$ reaction; the TS is at $s = 0$, and the reactant CH_3CHO and products $CH_4 + CO$ correspond to the $s < 0$ and $s > 0$ regions, respectively, and the zero point of the potential energy is set to the total energy of CH_3CHO. It is interesting to note that the potential energy does not converge to zero in the reactant region, indicating that the IRC connects with another CH_3CHO that is higher in energy than the one calculated in the present study. This CH_3CHO is rotated around the CC axis by 60° from the present one displayed in Figure 1, and is a TS between conformers. Therefore the reactant CH_3CHO should rotate around the CC axis when the $CH_3CHO \rightarrow CH_4 + CO$ reaction occurs. Although the effect of this IRC character on the reaction dynamics is of considerable interest, this is not directly relevant to the present photodissociation reaction, because the reactant CH_3CHO must be in quite high vibrational levels and potential features around and after the TS are considered more important to the dynamics.

B. A Sample Trajectory. In this subsection, one of the trajectories is arbitrarily chosen as a sample and its characteristics are discussed. Figures 3a and 3b show changes in potential energy and geometrical parameters, respectively, as a function of time. Note that the zero point of the potential energy is set to the total energy of the TS. It is seen that the potential energy decreases to ~ −80 kcal mol^{-1} in the first 15 fs and, after that, it regularly changes between −80 and −20 kcal mol^{-1}. It is interesting that the narrow and wide peaks are seen to alternately repeat. It is clear from Figure 3b that this behavior of the potential energy is mostly ascribed to the remarkable change in the C_1H_1 bond length. Note that the numbering for the atoms is denoted in the TS geometry in Figure 1. It is readily expected from the vector of the imaginary vibration of the TS given in Figure 1 that the C_1H_1 bond is highly vibrationally excited in the product region. The maximum length of the C_1H_1 bond is ~1.7 Å and the minimum length is ~0.8 Å. It is seen that when the C_1H_1 bond takes the maxima, the potential energy is at the tops of wide peaks, and when the bond takes the minima, it is at the tops of narrow peaks. This is because the equilibrium C_1H_1 bond length is ~1.1 Å and, consequently, it takes longer time for the bond to change from the equilibrium value, reach the maximum, and return to the equilibrium, than for it to change in the reverse direction, reach the minimum, and return to the equilibrium.

The C_1C_2O angle is seen to change from 120° to 0° in ~40 fs, indicating that the product CO is rotationally excited and it takes ~120 fs for the CO to rotate 360°. The C_2O bond exhibits almost no change, indicating that the product CO is vibrationally not excited. The C_1C_2 bond shows a monotonic increase and reaches 6 Å in ~75 fs.

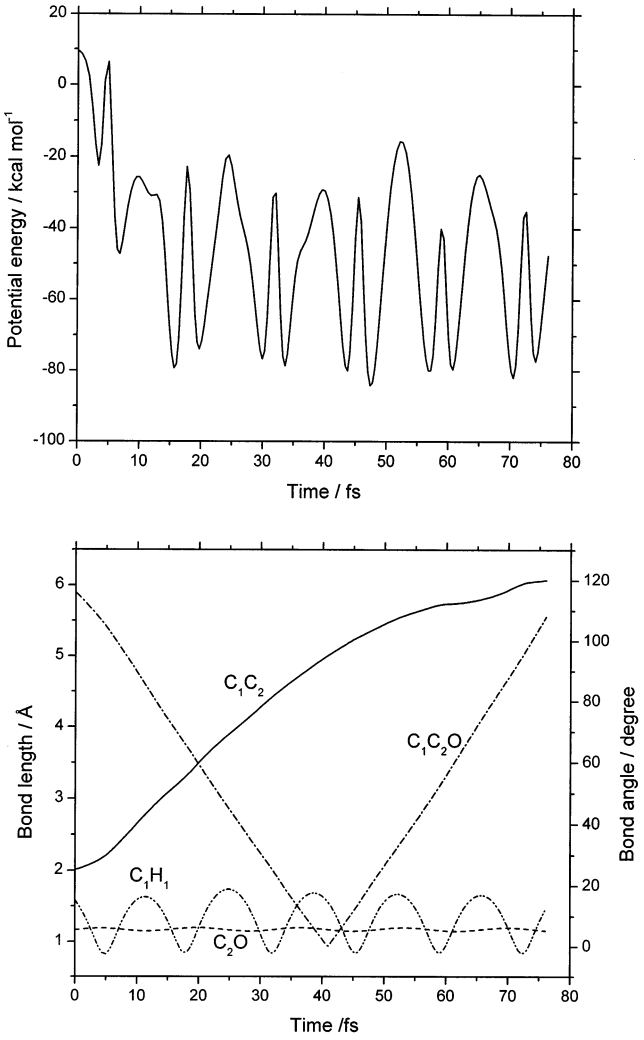

Figure 3. Changes in (a) potential energy and (b) geometrical parameters as a function of time.

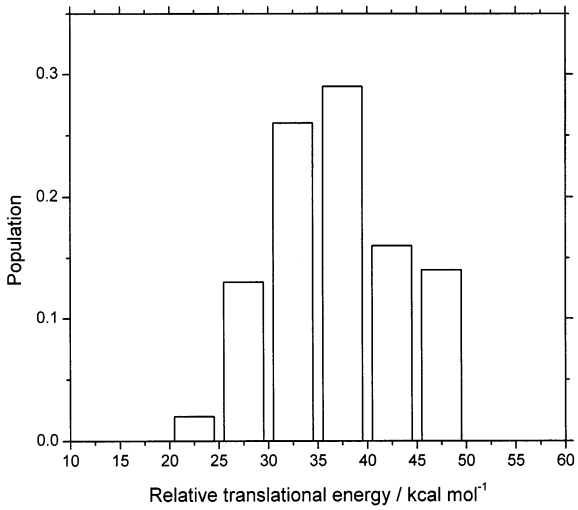

Figure 4. Relative translational energy distribution of the products CH_4 and CO.

C. Energy and State Distributions and Vector Correlation. Figure 4 shows the distribution of the relative translational energy of the products CH_4 and CO for the calculated 100 trajectories. The population of the relative translational energy is seen to be the largest around 35−40 kcal mol^{-1}, and its

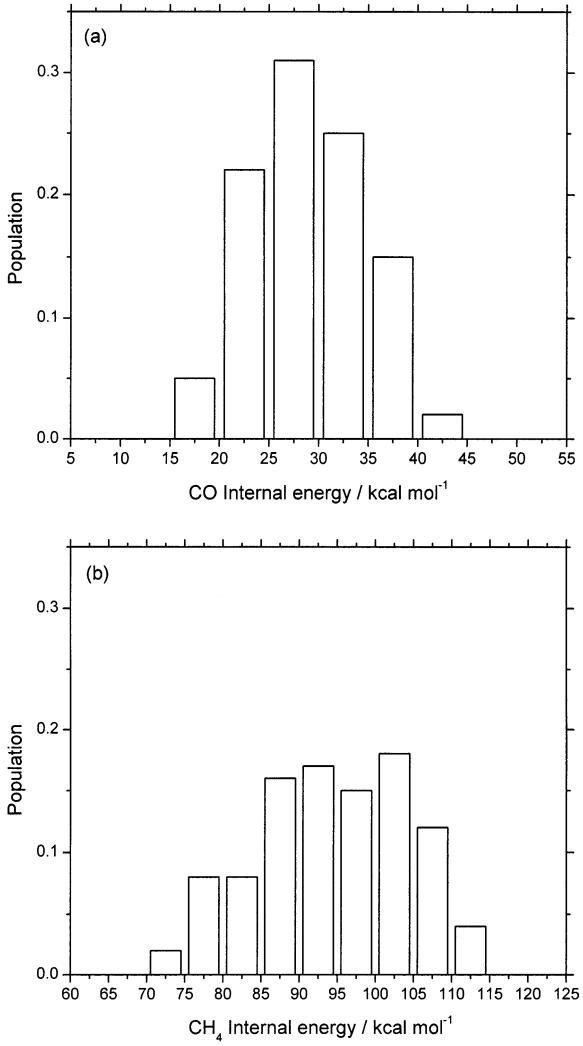

Figure 5. Internal energy distributions for the products: (a) CO; (b) CH_4.

average is 36.9 kcal mol^{-1}. At the starting point of the trajectories, kinetic energy of ∼35 kcal mol^{-1} was added to the reaction coordinate. Since the reverse barrier height with the ZPE correction was calculated to be ∼95 kcal mol^{-1} at the RMP2(full)/cc-pVDZ level (see Table 3), the available energy for the total system at the exit region is ∼130 kcal mol^{-1}. In short, one can state that 28% of the available energy transfers to the relative translational energy and the rest to the internal energies of CH_4 and CO. Figure 5 displays the distribution of the product internal energy: (a) CO and (b) CH_4. The CO internal energy exhibits a sharp distribution and the population is the largest around 25−30 kcal mol^{-1}, while the CH_4 internal energy has a wide distribution and the population is large in the region 85−110 kcal mol^{-1}. The averages of the CO and CH_4 internal energies are 28.8 and 94.4 kcal mol^{-1}. Subtracting the ZPEs of CO and CH_4, one obtains the average energies to be 25.8 and 65.8 kcal mol^{-1}, which are 20 and 51% of the available energy. The reason CH_4 has larger internal energy and broader energy distribution than CO is that CH_4 has larger degrees of freedom and the vector of the reaction coordinate at the TS will cause a highly excited vibrational motion of a CH bond of the CH_4 product. It is noted that the present result for the product energy distributions is in contrast to the theoretical[3i,j] and experimental[2b] results for the $H_2CO \rightarrow H_2 + CO$ reaction. The average ratio of the relative translational energy to the total available energy was calculated to be ∼60% by

Sung and Kim[3i] and ~70% by Li et al.[3j] and was measured to be ~65% by Ho et al.;[2b] these values are significantly larger than the present prediction for the CH_3CHO photodissociation. This is probably because the H_2CO system has much smaller degrees of freedom and the vector of the reaction coordinate at the TS is mainly composed of the relative translation of H_2 and CO.

The distributions of the CO rotational and vibrational quantum numbers are shown in Figure 6, parts a and b, respectively. In obtaining the quantum numbers, we assumed that the coupling between rotation and vibration is negligible. As expected from the vector of the imaginary mode at the TS and the analysis of the sample trajectory, the CO product is highly rotationally hot and vibrationally cold. The distribution of the CO rotational quantum number is seen to be the largest around 70−75 and its average is 68.2. It has been predicted that 85% of the CO vibrational quantum number is 0. These computational results qualitatively agree with the observation of Gherman et al.[4n] that no vibrationally excited CO was detected and the rotational temperature was 1300 ± 90 K. In the present work. we have predicted that 15% of the product CO is in the first vibrationally excited state and found that the rotational temperature could not be determined. This is probably because the chosen initial condition is somewhat artificial; the excess energy at the TS was given only to the reaction coordinate. Other reasons may be that the trajectories were run in a very short time, i.e., ~80 fs, and that the total number of the trajectories was not sufficient, i.e., 100.

It is also of interest to compare with the computational results[3i,j] for the $H_2CO \rightarrow H_2 + CO$ reaction. The calculated product state distributions for this reaction and the $CH_3CHO \rightarrow CH_4 + CO$ reaction are qualitatively quite similar. It was predicted that the product CO for the H_2CO photodissociation is vibrationally cold and rotationally hot; the average of the vibrational quantum number is ~0.1 and that of the rotational quantum number is ~45.[3j] On the other hand the product H_2 was calculated to be vibrationally hot and rotationally cold; the average of the vibrational quantum number is ~1.2, and that of the rotational quantum number is only ~3.[3j] These data are comparable with experiment.[2c,d] The H_2 vibrational excitation corresponds to the CH vibrational excitation in the product CH_4 in the CH_3CHO photodissociation. It seems that the calculated average CO rotational quantum number, 68.2, for the CH_3CHO photodissociation is about one and a half times larger than that for H_2CO. Note that, in the present calculations, kinetic energy of ~35 kcal mol^{-1} was added to the reaction coordinate and the total available energy is ~130 kcal mol^{-1}, while in the H_2CO calculations[3j] kinetic energy of 5 kcal mol^{-1} was added to the reaction coordinate, thus the available energy is about 100 kcal mol^{-1}. It is obvious that the average CO rotational quantum number strongly depends on the total available energy. Assuming that the percentage of energy partitioning does not sensitively depend on the total available energy, we will predict the average CO rotational quantum number to be ~60 if we add kinetic energy of 5 kcal mol^{-1} instead of 35 kcal mol^{-1} to the reaction coordinate at the TS in the trajectory calculations. This means that the rotational state of the product CO from the CH_3CHO is more highly excited than that of the CO from the H_2CO photodissociation.

Figure 7 shows the vector correlations between the products rotational angular momentum vectors **J** and the relative translational vector $\mathbf{v}_{rel}$: (a) $\mathbf{J}_{CO}$ and $\mathbf{v}_{rel}$; (b) $\mathbf{J}_{CH_4}$ and $\mathbf{v}_{rel}$. It is seen in Figure 7a that the angle between $\mathbf{J}_{CO}$ and $\mathbf{v}_{rel}$ has a sharp distribution around 90°, indicating that the CO rotational axis

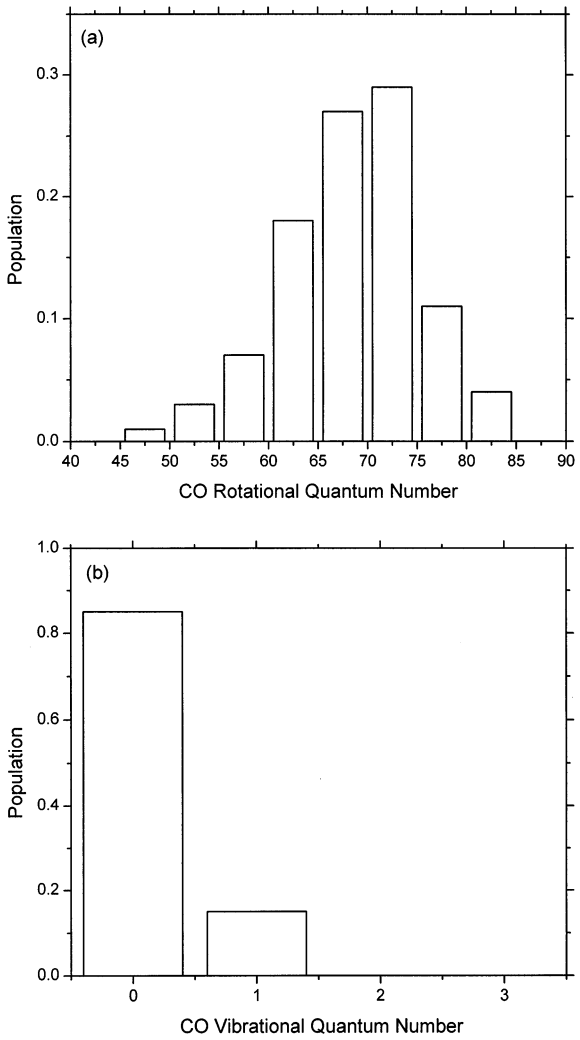

Figure 6. Product CO state distributions: (a) rotational quantum number; (b) vibrational quantum number.

tends to keep orthogonal to $\mathbf{v}_{rel}$. A broader distribution has been predicted in the angle between $\mathbf{J}_{CH_4}$ and $\mathbf{v}_{rel}$, as shown in Figure 7b, which is probably because CH_4 has larger degrees of freedom. Figure 8 depicts the vector correlations between **J** and the orbital angular momentum vector of the products **L**: (a) $\mathbf{J}_{CO}$ and **L**; (b) $\mathbf{J}_{CH_4}$ and **L**. It is seen in Figure 8a that the angle between $\mathbf{J}_{CO}$ and **L** has a sharp distribution near 180°, meaning that the product CO tends to rotate in the reverse direction of the orbital motion of the products. In Figure 8b is seen a broader distribution in the angle between $\mathbf{J}_{CH_4}$ and **L** around 0°. This indicates that the product CH_4 tends to rotate in the same direction as the orbital motion, but the tendency is not so strong. Figure 9 shows the vector correlation between $\mathbf{J}_{CO}$ and $\mathbf{J}_{CH_4}$; it is seen that the distribution is rather broad, but it is concentrated around 180°. This means that the products CH_4 and CO tend to rotate in the reverse direction, which is expected from the vector of the imaginary frequency of the TS shown in Figure 1.

In the present trajectory calculations the excess energy of ~35 kcal mol^{-1} at the TS was distributed only to the reaction coordinate. This is actually an artificial way of modeling the unimolecular dissociation that begins with the $S_1 \rightarrow S_0$ IC, because the excess energy at the TS is expected to impartially flow into all vibrational modes including the reaction coordinate. An improved simulation can be done by using the microcanonical ensemble for the initial condition. The improved

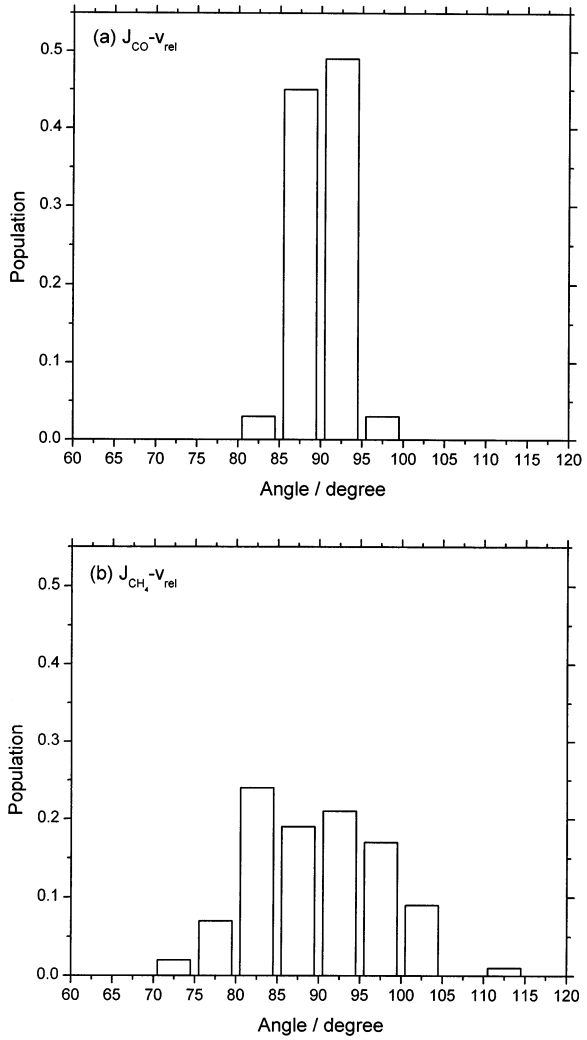

Figure 7. Vector correlations between the products rotational angular momentum vectors **J** and the relative translational vector $\mathbf{v}_{rel}$: (a) $\mathbf{J}_{CO} - \mathbf{v}_{rel}$; (b) $\mathbf{J}_{CH_4} - \mathbf{v}_{rel}$.

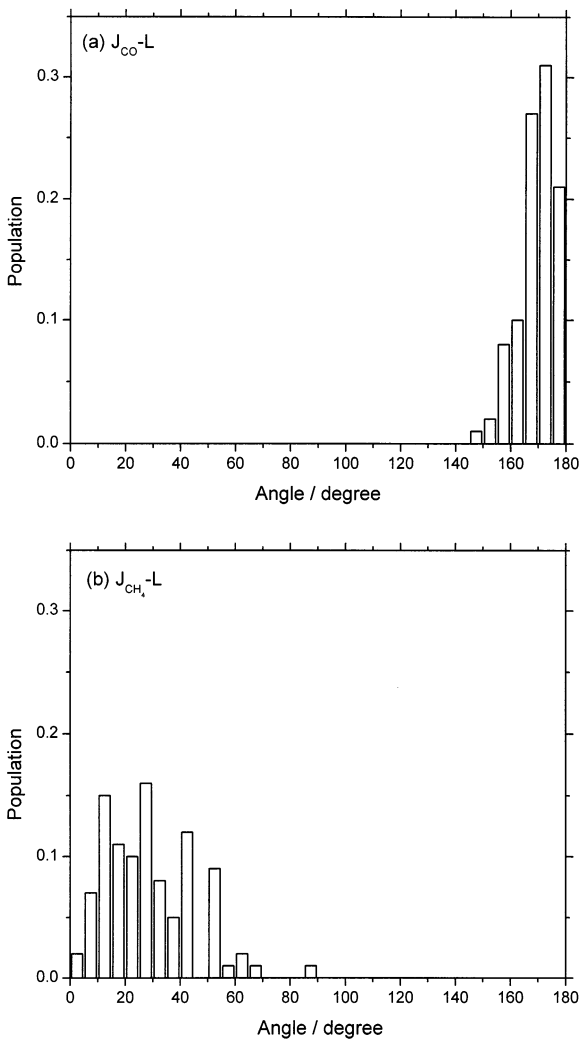

Figure 8. Vector correlations between **J** and the orbital angular momentum vector of the products **L**: (a) $\mathbf{J}_{CO} - \mathbf{L}$; (b) $\mathbf{J}_{CH_4} - \mathbf{L}$.

trajectory calculations would predict the CO rotational and vibrational state distributions that agree better with experiment, as mentioned above. We do not think, however, that the error due to the artifact in the initial condition is quite serious, because the reverse barrier height is very high and the molecule will gain another ~95 kcal mol^{-1} during dissociation.

4. Conclusion

In this study, using the direct ab initio molecular dynamics method, we have calculated a total of 100 trajectories for the photodissociation, $CH_3CHO \rightarrow CH_4 + CO$, on the S_0 potential surface. The employed ab initio level was RMP2(full)/cc-pVDZ, which was confirmed to be sufficiently reliable for describing the reaction dynamics by comparing with results obtained at higher levels of theory and with experiment. Analysis of a sample trajectory revealed that the change in the potential energy of the total system is almost ascribed to a CH bond vibration in the product CH_4. It was calculated that the energy distributions for the relative translational energy, the CO internal energy, and the CH_4 internal energy are 28, 20, and 51%, respectively. The high percentage of the CH_4 internal energy may be explained by the large degree of freedom of CH_4 and by the fact that the vector of the reaction coordinate at the TS will cause a highly excited vibrational motion of a CH bond of CH_4. It was predicted that the product CO is highly rotationally excited but vibrationally almost not excited; on average, the rotational and vibrational quantum numbers were 68.2 and 0.15, respectively, which qualitatively agrees with experiment. The vector correlation between the products rotational angular momentum vectors showed that the products CH_4 and CO tend to rotate in the reverse direction, which is expected from the vector of the imaginary frequency of the TS.

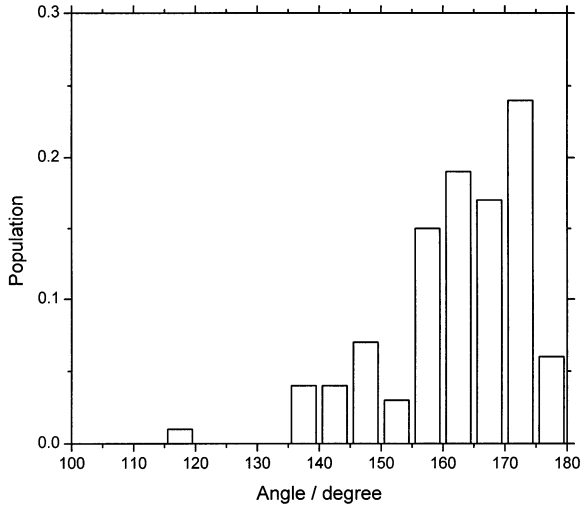

Figure 9. Vector correlation between $\mathbf{J}_{CO}$ and $\mathbf{J}_{CH4}$.

To better simulate the actual dissociation dynamics, the initial conditions should be more properly set up. The improved trajectory calculations would predict the product energy and state distributions that agree better with experiment. Such calculations are now underway in our laboratory.

Acknowledgment. Y.K. thanks Prof. H. B. Schlegel and Dr. X. Li for their helpful advice on using the trajectory code implemented in Gaussian 98.

References and Notes

(1) Calvert, J. G.; Pitts, J. N., Jr. *Photochemistry*; Wiley: New York, 1966.

(2) (a) Houston, P. L.; Moore, C. B. *J. Chem. Phys.* **1976**, *65*, 757. (b) Ho, P.; Bamford, D. J.; Buss, R. J.; Lee, Y. T.; Moore, C. B. *J. Chem. Phys.* **1982**, *76*, 3630. (c) Debarre, D.; Lefrebvre, M.; Pealat, M.; Taran, J.-P. E. *J. Chem. Phys.* **1985**, *83*, 4476. (d) Bamford, D. J.; Filseth, S. V.; Foltz, M. F.; Hepburn, J. W.; Moore, C. B. *J. Chem. Phys.* **1985**, *82*, 3032. (e) Guyer, D. R.; Polik, W. F.; Moore, C. B. *J. Chem. Phys.* **1986**, *84*, 6519. (f) Butenhoff, T. J.; Carleton, K. L.; Moore, C. B. *J. Chem. Phys.* **1990**, *92*, 377. (g) van Zee, R. D.; Foltz, M. F.; Moore, C. B. *J. Chem. Phys.* **1993**, *99*, 1664.

(3) (a) Goddard, J. D.; Schaefer, H. F., III. *J. Chem. Phys.* **1979**, *70*, 5117. (b) Harding, L. B.; Schlegel, H. B.; Krishnan, R.; Pople, J. A. *J. Phys. Chem*. **1980**, *84*, 3394. (c) Dupuis, M.; Lester, W. A.; Lengsfield, B. H.; Liu, B. *J. Chem. Phys.* **1983**, *79*, 6167. (d) Feller, D.; Dupuis, M.; Garret, B. C. *J. Chem. Phys.* **2000**, *113*, 218. (e) Schinke, R. *Annu. Rev. Phys. Chem*. **1988**, *39*, 39. (f) Miller, W. H.; Hernandez, R.; Handy, N. C.; Jayatilaka, D.; Willetts, A. *Chem. Phys. Lett*. **1990**, *172*, 62. (g) Chen, W.; Hase, W. L.; Schlegel, H. B. *Chem. Phys. Lett*. **1994**, *228*, 436. (h) Peslherbe, G. H.; Hase, W. L. *J. Chem. Phys.* **1996**, *104*, 7882. (i) Sung, B. J.; Kim, M. S. *J. Chem. Phys*. **2000**, *113*, 3098. (j) Li, X.; Millam, J. M.; Schlegel, H. B. *J. Chem. Phys*. **2000**, *113*, 10062.

(4) (a) Hansen, D. A.; Lee, E. K. C. *J. Chem. Phys*. **1975**, *63*, 3272. (b) Horowitz, A.; Kershner, C. J.; Calvert, J. G. *J. Phys. Chem*. **1982**, *86*, 3094. (c) Horowitz, A.; Calvert, J. G. *J. Phys. Chem*.**1982**, *86*, 3105. (d) Speiser, S.; Pfeiffer, W. F.; Atkinson, G. H. *Chem. Phys. Lett*. **1982**, *93*, 480. (e) Noble, M.; Lee, E. K. C. *J. Chem. Phys*. **1984**, *80*, 134. (e) Noble, M.; Lee, E. K. C. *J. Chem. Phys*. **1984**, *81*, 1632. (f) Ohta, N.; Baba, H. *J. Phys. Chem*. **1986**, *90*, 2654. (g) Kono, T.; Takayanagi, M.; Nishiya, T.; Hanazaki, I. *Chem. Phys. Lett*. **1993**, *201*, 166. (h) Kono, T.; Takayanagi, M.; Hanazaki, I. *J. Phys. Chem*. **1993**, *97*, 12793. (i) Terentis, A. C.; Stone, M.; Kable, S. H. *J. Phys. Chem*. **1994**, *98*, 10802. (j) Lee, S.-H.; Chen, I.-C. *J. Chem. Phys.* **1996**, *105*, 4597. (k) Gejo, T.; Bitto, H.; Huber, J. R. *Chem. Phys. Lett*. **1996**, *261*, 443. (l) Lee, S.-H.; Chen, I.-C. *Chem. Phys.* **1997**, *220*, 175. (m) Leu, G.-H.; Huang, C.-L.; Lee, S.-H.; Lee, Y.-C.; Chen, I.-C. *J. Chem. Phys.* **1998**, *109*, 9340. (n) Gherman, B. F.; Friesner, R. A.; Wong, T.-H.; Min, Z.; Bersohn, R. *J. Chem. Phys.* **2001**, *114*, 6128.

(5) (a) Yadav, J. S.; Goddard, J. D. *J. Chem. Phys*. **1986**, *84*, 2682. (b) Smith, B. J.; Nguyen, M. T.; Bouma, W. J.; Radom, L. *J. Am. Chem. Soc*. **1991**, *113*, 6452. (c) Martell, J. M.; Yu, H.; Goddard, J. D. *Mol. Phys*. **1997**, *92*, 497. (d) King, R. A.; Allen, W. D.; Schaefer, H. F., III. *J. Chem. Phys*. **2000**, *112*, 5585.

(6) (a) Head-Gordon, M.; Pople, J. A.; Frisch, M. J. *Chem. Phys. Lett.* **1988**, *153*, 503. (b) Frisch, M. J.; Head-Gordon, M.; Pople, J. A. *Chem. Phys. Lett.* **1990**, *166*, 275. (c) Frisch, M. J.; Head-Gordon, M.; Pople, J. A. *Chem. Phys. Lett.* **1990**, *166*, 281.

(7) Dunning, T. H., Jr. *J. Chem. Phys.* **1989**, *90*, 1007.

(8) (a) Krishnan, R.; Pople, J. A. *Int. J. Quantum Chem.* **1978**, *14*, 91. (b) Krishnan, R.; Frisch, M. J.; Pople, J. A. *J. Chem. Phys.* **1980**, *72*, 4244.

(9) Pople, J. A.; Head-Gordon, M.; Raghavachari, K. *J. Chem. Phys.* **1987**, *87*, 5968.

(10) (a) Fukui, K. *J. Phys. Chem.* **1970**, *74*, 4161. (b) Gonzalez, C.; Schlegel, H. B. *J. Chem. Phys.* **1989**, *90*, 2154. (c) Gonzalez, C.; Schlegel, H. B. *J. Phys. Chem.* **1990**, *94*, 5523.

(11) Frisch, M. J.; Trucks, G. W.; Schlegel, H. B.; Scuseria, G. E.; Robb, M. A.; Cheeseman, J. R.; Zakrzewski, V. G.; Montgomery, J. A., Jr.; Stratmann, R. E.; Burant, J. C.; Dapprich, S.; Millam, J. M.; Daniels, A. D.; Kudin, K. N.; Strain, M. C.; Farkas, O.; Tomasi, J.; Barone, V.; Cossi, M.; Cammi, R.; Mennucci, B.; Pomelli, C.; Adamo, C.; Clifford, S.; Ochterski, J.; Petersson, G. A.; Ayala, P. Y.; Cui, Q.; Morokuma, K.; Malick, D. K.; Rabuck, A. D.; Raghavachari, K.; Foresman, J. B.; Cioslowski, J.; Ortiz, J. V.; Baboul, A. G.; Stefanov, B. B.; Liu, G.; Liashenko, A.; Piskorz, P.; Komaromi, I.; Gomperts, R.; Martin, R. L.; Fox, D. J.; Keith, T.; Al-Laham, M. A.; Peng, C. Y.; Nanayakkara, A.; Gonzalez, C.; Challacombe, M.; Gill, P. M. W.; Johnson, B.; Chen, W.; Wong, M. W.; Andres, J. L.; Gonzalez, C.; Head-Gordon, M.; Replogle, E. S.; Pople, J. A. *Gaussian 98*, Revision A.7; Gaussian, Inc.: Pittsburgh, PA, 1998.

(12) (a) Millam, J. M.; Bakken, V.; Chen, W.; Hase, W. L.; Schlegel, H. B. *J. Chem. Phys.* **1999**, *111*, 3800. (b) Bakken, V.; Millam, J. M.; Schlegel, H. B. *J. Chem. Phys*. **1999**, *111*, 8773.

(13) Kilb, R. W.; Lin, C. C.; Wilson, E. B., Jr. *J. Chem. Phys*. **1957**, *26*, 1695.

(14) Afeefy, H. Y.; Liebman, J. F.; Stein, S. E. "Neutral Thermochemical Data" in *NIST Chemistry WebBook, NIST Standard Reference Database Number 69*; Linstrom, P. J., Mallard, W. G., Eds.; July 2001, National Institute of Standards and Technology, Gaithersburg, MD, 20899 (http://webbook.nist.gov).